Correcting for non-periodic behaviour in perturbative experiments: application to heat pulse propagation and modulated gas-puff experiments

Correcting for non-periodic behaviour in perturbative experiments: application to heat pulse propagation and modulated gas-puff experiments

M. van Berkel[1], R. J. R. van Kampen[1,2], G. Vandersteen[3], T. Kobayashi[4], T. Ravensbergen[1,2], H. Igami[4], J. T. Lammers[2,5], G. W. Oosterwegel[1,5], C. Galperti[6], F. Felici[6], M. R. de Baar[1,2], the LHD Experiment Group, and the TCV Team*

[1]DIFFER - Dutch Institute for Fundamental Energy Research, PO Box 6336, 5600HH Eindhoven, The Netherlands
[2]Eindhoven University of Technology, Dept. of Mechanical Engineering, Control Systems Technology Group, PO Box 513, 5600MB Eindhoven, The Netherlands
[3]Vrije Universiteit Brussel (VUB), Dept. of Fundamental Electricity and Instrumentation, Pleinlaan 2, 1050 Brussels, Belgium
[4]National Institute for Fusion Science, 322-6 Oroshi-cho, Toki-city, Gifu, 509-5292, Japan
[5]Eindhoven University of Technology, Dept. of Physics, Science & Technology of Nuclear Fusion, PO Box 513, 5600MB Eindhoven, The Netherlands
[6]École Polytechnique Fédérale de Lausanne (EPFL), Swiss Plasma Center (SPC), CH-1015 Lausanne, Switzerland
*See author list of S. Coda et al. 2019 Nucl. Fusion 59 112023
https://doi.org/10.1088/1741-4326/ab25cb

Abstract. This paper introduces a recent innovation in dealing with non-periodic behavior often referred to as transients in perturbative experiments. These transients can be the result from unforced response due to the initial condition and other slow trends in the measurement data and are a source of error when performing and interpreting Fourier spectra. Fourier analysis is particularly relevant in system identification used to build feedback controllers and the analysis of various pulsed experiments such as heat pulse propagation studies. The basic idea behind the methodology is that transients are continuous complex-valued smooth functions in the Fourier domain which can be estimated from the Fourier data. Then, these smooth functions can be subtracted from the data such that only periodic components are retained. The merit of the approach is shown in two experimental examples, i.e., heat pulse propagation (core transport analysis) and radiation front movement due to gas puffing in the divertor. The examples show that the quality of the data is significantly improved such that it allows for new interpretation of the results even for non-ideal measurements.

Submitted to: *Plasma Phys. Contr. Fusion*

1. Introduction

Perturbative or excitation experiments are a standard tool to study, determine, and validate dynamic models used to study physics and develop feedback controllers. In fusion, these experiments are performed for virtually every actuator that can vary in time and of which a resulting perturbed physics quantity can be observed varying in time [1, 2, 3]. Examples are perturbations induced by neutral beam injection [4], ion cyclotron excitation [5], electron cyclotron resonance heating (ECRH) [6, 7, 8, 9] but also other actuators such as gas puffing [10], pellet injection [11], and magnetic perturbations induced by coils [12]. These perturbations induce time variations in various quantities such as temperature, density, and current; are used to build, quantify, and assess dynamic models of, e.g., transport, impedance, and systems to be PID-controlled.

Especially, for the development of controllers, the estimation of transfer functions using perturbations is particularly interesting. For example, MHD control transfer functions are used to develop controllers for the (mechanical) gyrotron launcher [13]. Moreover, the transfer functions also describe the relationship between heating or current drive with respect to magnetic island width [14] and sawtooth period [15], which are mainly derived theoretically.

The pure perturbation measurement is, however, almost always disturbed by other phenomena, e.g., the system not being in equilibrium, drifts (also called trends), and changes in the measured quantities not related to the induced perturbation. These contributions are called transients and are an error contribution when analyzing perturbative experiments. This is a well-known problem and the standard approaches to deal with such error contribution are detrending (drift correction) and windowing (spectral leakage correction) [16]. However, it is well known that detrending removes polynomial (mostly linear) trends in the time evolution [16, 17] and that windowing itself is introducing spectral leakage and is subject to a trade-off [18, 19]. Hence, both can be useful but are not ideal. Therefore, modern techniques have been developed which attempt to separate within the measurement the transients from the actual perturbation using the smooth nature of transients [20]. These techniques allow the removal of arbitrary trend shapes and avoid self-introduced spectral leakage.

The idea behind new trend removal techniques is that the perturbations used to study the plasma are non-smooth (spikes) in the frequency domain, whereas transients have a smooth contribution over a large frequency range. To understand this better, consider the spectrum of a block wave modulation versus that of a trend. The contributions of the block-wave modulation of regular period are concentrated at a few frequencies whereas that of the drift/trend spreads over frequency as it is not described by a specific sinusoid but by a large sum of sinusoids dominating at low frequencies.

The method to be used for separation trends from perturbation depends on the specific information available such as a reference signal (noiseless) or knowledge which specific frequencies are perturbed. Moreover, a choice needs to be made how to approximate the smooth contribution due to transients. Two popular approximations are using local polynomials (LPM) and rationals of local polynomials (LRM). The LPM is generally used in case of smooth dynamics whereas in case of resonances the LRM is the preferred choice. In this work, only the LPM is used because we do not expect any resonances. Moreover, as the merit over detrending and windowing of this methodology has been shown in many examples in the literature, we refer to these examples [21, 22, 23] rather than showing this merit again. Instead, the merit of this approach will be shown for two rather different experimental nuclear fusion examples: 1) heat pulse propagation using electron cyclotron heating as perturbation and 2) gas puff modulation to change the C-III emission front.

The article is organised as follows. In Sec. 2, the local polynomial method is explained. Then, two experimental examples are worked out. In Sec. 3, a heat pulse propagation experiment for physics study is shown for the Large Helical Device and in Sec. 4 the application to movement of the C-III emission front using gas-puffing is shown for feedback control development on TCV. We conclude with a discussion in Sec. 5.

2. LPM: Local polynomial method

This paper describes how to remove transients using the local polynomial method. This section briefly discusses the theory behind the local polynomial method [24, 25].

2.1. Theoretical background

The philosophy of the local polynomial method [24, 25] (LPM) is that the spectral representation of signals can be decomposed into contributions with different characteristics. These different characteristics are 1) having a smooth spectral representation; 2) having systematic contributions; 3) are stochastic. By separating these components the signal can be decomposed and eventually some components can be compensated.

To better understand the operation of the LPM, consider that a signal

$$x(t) = x_{tran}(t) + x_{per}(t) + x_n(t), \tag{1}$$

where $x_{tran}(t)$ represents a transient signal (non-steady-state behavior, slow trend), $x_{per}(t)$ a periodic signal with periodic T ($x_{per}(t) = x_{per}(t+T)$) (periodic excitation and the response of linear and a large class of (non-)linear systems), and $x_n(t)$ the realization of an additive noise source (filtered noise).

Consider the (complex-valued) discrete Fourier transform (DFT) of the equidistantly time-sampled $x(t)$

$$X(f) = \mathcal{F}(x(t)). \tag{2}$$

The spectrum can then be written as

$$X(f) = X_{tran}(f) + X_{per}(f) + X_n(f), \tag{3}$$

where $X_{tran}(f) = \mathcal{F}(x_{tran}(t))$ is the transient spectrum, $X_{per}(f) = \mathcal{F}(x_{per}(t))$ the periodic spectrum, and $X_n(f) = \mathcal{F}(x_n(t))$ the noise spectrum.

Transient spectrum $X_{tran}(f)$ A transient spectrum has a smooth complex-valued function in the frequency domain and hence can be represented over a small frequency range using a polynomial function (hence the name local polynomial). This can easily be understood by noting that a transient signal originates from an (arbitrary) initial state, which is then shaped by the system's response induced by the (deterministic) model equations. Hence, although a transient is an arbitrary realisation due to the random initial states, its frequency dynamics is shaped by the (deterministic) frequency response functions of the system. Hence, a transient signal has a smooth function in the spectral domain.

The leakage effect introduced by the DFT over a finite time window can also be considered as a kind of transient effect. Consider therefore that a time-windowed signal $x_T(t)$ with a rectangular window of length T is made by

$$x_T(t) = x(t)s(t) - x(t)s(t-T), \tag{4}$$

with $s(t)$ the Heaviside step function (0 for negative t, 1 otherwise). In this case $x(t)s(t)$ can be considered as a regular transient response and hence has a smooth complex-valued spectrum. Hence, $x(t)s(t-T)$ and $x_T(t)$ also have a smooth complex-valued spectrum.

It is an important observation that spectral leakage introduced by applying finite (rectangular) time windows can be modelled for a small frequency range using a polynomial in the frequency domain.

Another important effect that can be captured by such a transient spectrum is trends/drifts in the instrumentation, as these trends can also be considered as a kind of transient signal.

Periodic spectrum $X_{per}(f)$ If the Fourier spectrum is calculated of a (perfect) periodic signal and the number of periods are increased (with integers), then only non-zero contributions exist at specific individual frequencies, also known as bins, within the DFT spectrum: if n periods of sine or cosine components fit into the window, then there will only be a contribution to the n^{th}-bin. This enables the separation of transient from period signals as periodic signals only have contributions to the specific (isolated) frequencies, while the transient transient spectra have a smooth behavior.

The classical setting of identifying linear time-invariant systems makes use of multisine excitations which are sums of sinewaves at the set of (well selected) frequencies (bins), i.e.,

$$x_{per} = \sum_{k=1}^{N} A_k \cos 2\pi k f_0 + B_k \sin 2\pi k f_0. \tag{5}$$

When measuring a time window of n periods of such multisine, one expects $n-1$ zero contributions in between the excited frequencies (bins) or also called harmonics. These $n-1$ harmonics can be used to model the other signal (transient and noise).

Noise spectrum $X_n(f)$ A last type of contribution is the additive noise where it is known that under weak assumptions [24] a DFT transforms filtered white noise into zero-mean circularly-symmetric complex normal distributed noise (CCND) [26] and that this noise becomes independent over the different frequencies when the number of samples (and hence observation window) tends to infinity.

The noise variance as a function of the frequency can easily be estimated from the residual errors of the polynomial model estimated in a local small frequency band around the frequency of interest.

2.2. Existing extensions of the LPM

In this work, we only use the LPM. However, we want to point out that there are cases where

the LPM is inefficient in describing the system at hand. For instance, lightly damped systems have a frequency response that is inefficiently approximated by polynomials. This is due to resonances, that for instance can exist in the mechanical mirror control of a electron cyclotron resonance heating system [13]. Hence, in case of resonances, a rational function is more efficient to approximate the resonating behavior of the underlying lightly damped poles. This leads to the introduction of Local Rational Models (LRM) [27, 28, 29]. However, if the problem at hand is damped (no lightly damped poles), then there is no advantage in using this LRM. Another natural extension is to enable the measurement of the frequency response matrix of multiple-input multiple-output systems [30].

2.3. Standard implementations and extension to state-of-the-art

There exist many different versions and implementations of the local polynomial methodology. In this work, we base ourselves on the algorithms described [20]. For the LPM, in principle two methodologies are available: 1) using periodic excitation or perturbation which is adapted in this paper and 2) using a noiseless reference signal which is not necessarily periodic but should definitely not be smooth. The latter is important in cases where it is not possible to impose a pure periodic signal as excitation. In this paper, the aim in the first example (LHD) is to remove transient effects (originating from an initial condition, leakage or trends) on steady state measurements of a weakly nonlinear system (the plasma) excited by 2 periodic signals that both have harmonic components. If two signals are considered having a base frequency of $f_1 = n_1 f_0$ and of $f_2 = n_2 f_0$ results in a set of excited frequencies $\{kn_1\}$ for the first and $\{ln_2\}$ for the second excitation (for non-zero integers n_1, n_2, k, and l).

Applying the periodic signals at f_1 and f_2 to a weakly nonlinear system (Sec. 3) will generate inter-modulation frequencies. A weakly nonlinear system up to the third order (higher order generalizations are possible) results in additional frequency components, also known as inter-modulation components. A second order nonlinear behaviour will generate the set $\{|kn_1 \pm ln_2|\}$, while a third order generates $\{|2kn_1 \pm ln_2|\}$ and $\{|kn_1 \pm 2ln_2|\}$. Both have been implemented but third order non-linear contributions are generally significant smaller and can often be excluded.

Hence, the LPM method used is tuned to measure the inter-modulation distortion when exciting with a 2-tone excitation. This implies a more specific pruning of the lines which are used to model the transient and the periodic spectrum, leading to a better estimate of the transient. This transient estimate can then be removed from its contribution to the periodic harmonics under investigation. For the second example, we use the standard methodology for periodic signals [20]. As the local polynomial method is a standing method [20], we have not included a simulation example. Instead, we use to experimental examples for which we know approximately how the spectra should behave without transient errors. As the next two sections show, the LPM corrects the spectra correctly without including any knowledge in the algorithm of how the spectra behave.

3. Application of LPM to heat pulse propagation experiments

This section presents the results of applying the local polynomial method (LPM) to electron heat pulse propagation experiments performed at the Large Helical Device (LHD) which was applied but not explained in [31]. First, the experiment is introduced briefly including relevant device and discharge parameters. Then, the local polynomial method is applied and discussed for a specific user case. Finally, the method is applied to all spatial measurements revealing trends which are not visible in the original measurement data without correcting for transient errors using the LPM.

3.1. Experimental device and discharge information

The perturbation experiment presented in this section is shown in Fig. 1. It is measured in the Large Helical Device (LHD) which is a heliotron (stellarator type) with a major radius $R_{major} = 3.5 \sim 3.9$ m and effective (averaged) minor radius is $a_{99} = 0.6$ m [32]. The dimensionless radius is defined as $\rho = r_{eff}/a_{99}$ where r_{eff} is the effective radius [33]. The discharge shown in this section is an L-mode discharge with on-axis magnetic field of 2.75 T using two tangential co/counter neutral beams of total 10 MW (near zero beam driven current) and a line-averaged density of approximately $0.9 \cdot 10^{19}\,\mathrm{m}^{-3}$. As LHD is a heliotron-type machine, little macroscopic magneto-hydrodynamic instabilities such as sawteeth and neo-classical tearing modes disturb the measurements.

The presented experiment in Fig. 1 is different from standard perturbation experiments, in which the linear response is studied [1], as it is specifically designed to quantify the non-linear contributions. The non-linear contributions can be quantified by the amplitude of the Fourier coefficients at the inter-modulation frequencies, i.e., the sum and difference frequencies of two sources with a different modulation frequency in this case f_1 and f_2 [31, 34]. The amplitude of these coefficients is a measure for the non-linearity and the similarity between the sum $|f_1 + f_2|$ and difference $|f_1 - f_2|$ frequency can be

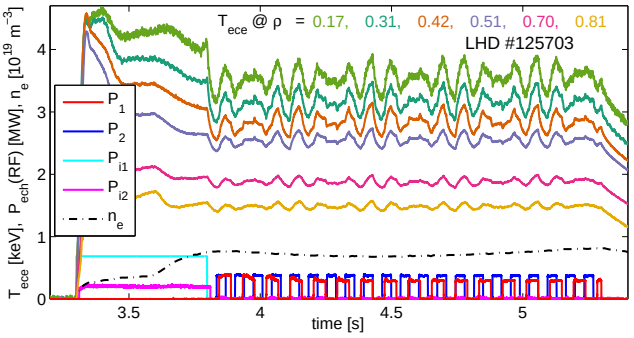

Figure 1. *color online* Discharge overview and device information (see for more details [31]). For the steady-state phase, the perturbation is applied using approximately 2×0.3 MW of injected electron wave power from the low magnetic field side using the horizontal port launchers called 2Oll for 154GHz 2nd X-mode (P_1) and 2Olr for 77GHz 1st O-mode (P_2) [35]. They are operated to create symmetric power (block-type) modulated EC waves which generate electron heat pulses and fundamental frequencies of $f_1 = 11.11$ Hz (P_1) and $f_2 = 14.29$ Hz (P_2) such that the joint period corresponds to 1.59 Hz. The deposition locations were chosen such that both are around $\rho = 0.2$.

used for determining what type of non-linearity is present [20]. The challenge is that these inter-modulation contributions at the specific sum and difference frequencies have by definition a smaller amplitude than the primary harmonic components f_1 and f_2. Moreover, as with most experiments in tokamaks, time-traces are rather short and in this case only two full joint periods could be measured. Hence, these harmonic components are more prone to errors such as noise and, specifically, transients. As was explained above, the transient is mainly a low frequent source of error, thus it particularly $|f_1 - f_2|$ needs to be corrected as it is most prone to transient errors.

The corresponding Fourier spectra to Fig. 1 at two spatial locations of the calibrated ECE-temperature measurements are presented in Fig. 2 (top) and Fig. 3 (top). In both figures, two main peaks are observed at $f_1 = 11.11Hz$ and $f_2 = 14.29Hz$. In total two joint periods (of f_1 and f_2) are measured in the window 4 - 5.26 s which corresponds to a frequency resolution of the DFT of approximately 0.79 Hz. These correspond to the modulation pattern of the two gyrotrons with duty cycle 50% shown in Fig. 1 (f_1 in red and f_2 in blue). If the response is weakly non-linear then small harmonic components are expected at $2f_1$, $2f_2$, and $|f_1 \pm f_2|$. However, what we observe in Fig. 2 (top) and Fig. 3 (top) is that due to the transient, the low-frequent part of the spectrum decays slowly without peaks clearly recognizable up to approximately 5 Hz. Consequently, the inter-modulation frequency at $|f_1 - f_2|$ cannot be distinguished from the transient. In the next sub-section, the LPM is applied to show that this component can be distinguished when the transient is removed.

3.2. LPM in detail (one spatial location)

For the removal of the transient particularly at $|f_1 - f_2|$ a modified local polynomial algorithm is used compared to the original LPM algorithm [24] for periodic data. The original algorithm uses the harmonic components surrounding the multiples of the modulation frequencies (f_1, f_2, and its multiples). The algorithm is extended by assuming in addition that the sum and difference frequencies can also have contributions due to the non-linearities as is the case. For all the other frequencies, it is assumed that the Fourier coefficients are a combination of noise and transients but specifically are not related to a periodic perturbation. This is for almost all perturbative experiments a reasonable assumption especially in controlled experiments as is the case here. Consequently, all these not perturbed frequencies in the spectrum can be used to estimate the transient at the inter-modulation frequencies and the directly perturbed harmonic components. Here, we chose a quadratic polynomial to be fitted through the surrounding non-perturbed harmonic components and estimate the transient at the interpolated complex value at the frequency of the inter-modulation. Therefore, it is assumed that in a small frequency region the noise is white, i.e., the variance is the same over the harmonics used to interpolate the inter-modulation frequencies. Moreover, the residual of the interpolation can be used to estimate the variance of the noise at the inter-modulation frequency [24]. Then, in the last step the transient is subtracted (in the complex plain) from the inter-modulation harmonic, thereby removing its contribution. This is shown in Fig. 2 (bottom) and Fig. 3 (bottom) for the difference inter-modulation frequency, i.e., $|f_1 - f_2| = 3.17$ Hz, at radial locations $\rho = 0.24$ and $\rho = 0.48$, respectively.

These figures show the Fourier coefficients of the four non-perturbed harmonics, i.e., 1.59, 2.38, 3.97, 4.76 Hz, surrounding the perturbed harmonic at 3.17 Hz. The four non-perturbed harmonics are only subject to the transient and noise. The transient is approximated by a quadratic function which is complex-valued (in red). This function is the local polynomial in the LPM. Then, at frequency 3.17, the contribution of the transient is approximated using interpolation. This value needs to be subtracted in the complex-plane from the measured (raw) Fourier coefficient. This results in a new value for the Fourier coefficient without the transient. Depending on the phase of the transient and the measured Fourier coefficient, the value of the corrected Fourier coefficient can decrease as shown in Fig. 2 or can increase as shown in Fig. 3 by the green crosses. Especially, at $\rho = 0.48$

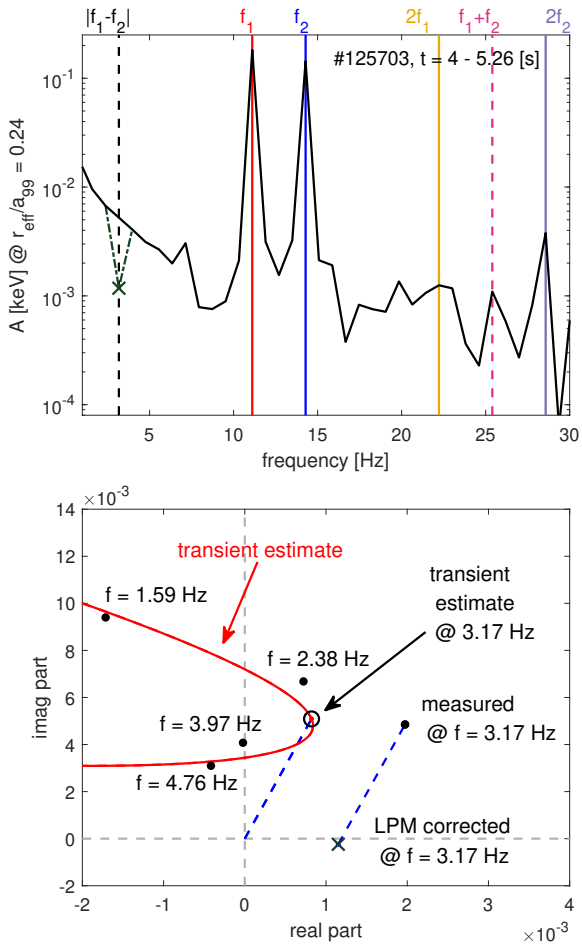

Figure 2. *color online* (top) The Fourier spectrum of the calibrated ECE-measurements at $\rho = 0.24$ (black). The solid vertical lines show the contributions at the perturbed harmonics. The dashed-dotted lines show the locations of the primary inter-modulations. The green cross at $|f_1 - f_2|$ shows the resulting amplitude of $|f_1 - f_2|$ after applying the local polynomial method. (bottom) Graphical representation of the local polynomial method with in red the (local) quadratic complex polynomial fitted through the surrounding non-perturbed frequency points. This allows for an estimate of the transient at the frequency belonging to $|f_1 - f_2|$. The distance in the complex-plane (blue dashed), i.e., the transient must be subtracted from the measured Fourier coefficient at that frequency. This results in the corrected Fourier coefficient (LPM corrected).

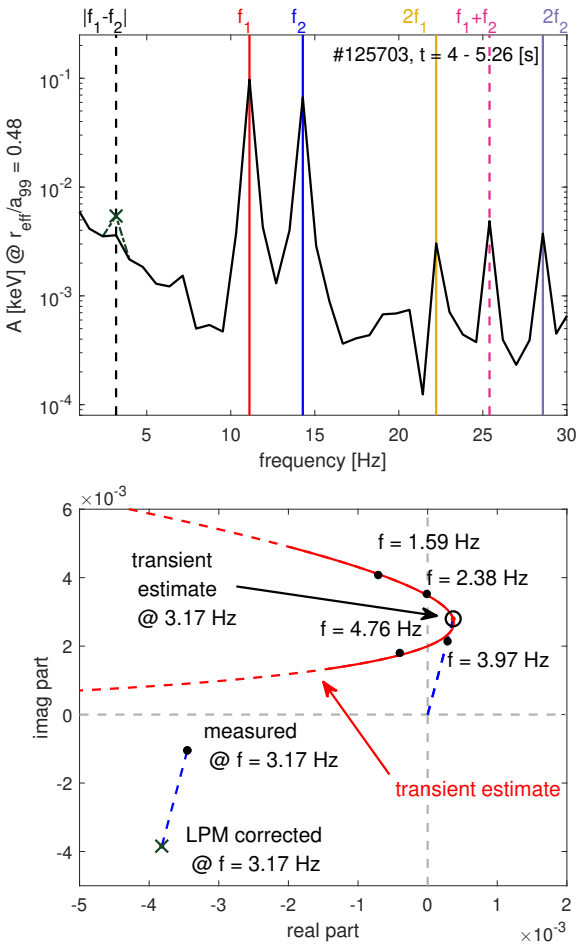

Figure 3. *color online* (top) The Fourier spectrum of the calibrated ECE-measurements at $\rho = 0.48$ (black). The solid vertical lines show the contributions at the perturbed harmonics. The dashed-dotted lines show the locations of the primary inter-modulations. The green cross at $|f_1 - f_2|$ shows the resulting amplitude of $|f_1 - f_2|$ after applying the local polynomial method. (bottom) Graphical representation of the local polynomial method with in red the (local) quadratic complex polynomial fitted through the surrounding non-perturbed frequency points. This allows for an estimate of the transient at the frequency belonging to $|f_1 - f_2|$. The distance in the complex-plane (blue dashed), i.e., the transient must be subtracted from the measured Fourier coefficient at that frequency. This results in the corrected Fourier coefficient (LPM corrected).

is the appearance of a strong harmonic component striking. This will be further analyzed and extended in the next subsection.

3.3. LPM applied over frequency for all spatial distributions

In the previous subsection, we have shown the result of the LPM at two specific spatial locations and only for the frequency $|f_1 - f_2|$. Here, we will analyze the effect of applying the LPM for all spatial locations and for all relevant harmonic components up to 30 Hz, which is shown in Fig. 4 (top).

First of all, recall that the LPM is applied independently at every spatial location and secondly it uses only the four harmonic components surrounding the perturbed harmonic to be corrected. As such no correlation between space and frequency is introduced by applying the LPM. Moreover, we chose to use a quadratic (parabolic) polynomial as is shown in Fig. 2 and in Fig. 3 such that four surrounding harmonics can be used. On the other hand, we also tested linear polynomials (not shown here). Although the result did

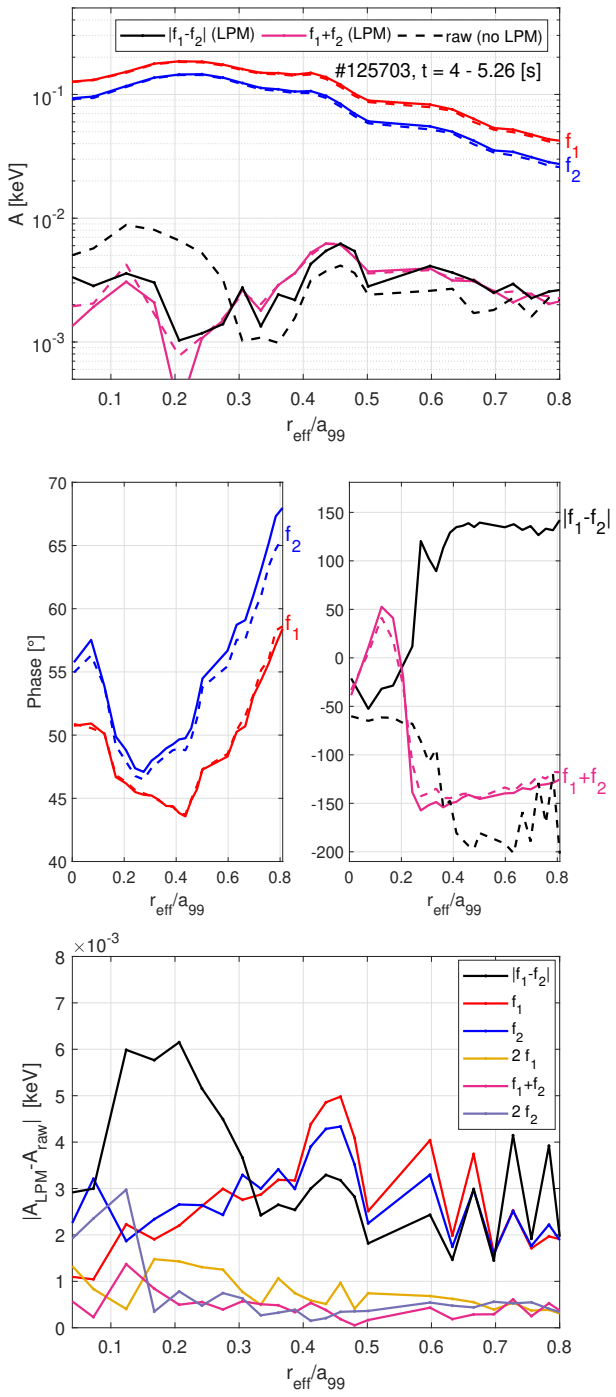

Figure 4. *color online* Profiles of the main harmonics as function of the spatial location. The solid lines show the estimates compensated with the LPM method, the dashed lines the (uncompensated) profiles. (top) Amplitude profiles (middle) Phase profiles. Note that the phase has been compensated with the source modulation phase for f_1 and f_2 but not for $|f_1 \pm f_2|$. Unlike the rest of the paper the phase in this figure is defined in terms of delay (negative phase) as is common in transport experiments. (bottom) The absolute error between the measured and LPM corrected amplitudes. Also the frequencies 2 f_1 and 2 f_2 are shown for completeness. Note that at low-frequencies the error is generally larger than at higher frequencies due to decay of transient as function of frequency.

change quantitatively, the result remains qualitatively the same. The degree of the polynomial (quadratic, cubic) and number of non-excited frequencies (those that do not contain a perturbation) used to fit the polynomial are for the user to decide.

If we now analyze the result in applying the quadratic LPM using four frequencies, we observe that the changes are most significant for $|f_1 - f_2|$ (for both amplitude and phase) and to a much lesser extend to f_1, f_2, and $|f_1 + f_2|$. Although it is unclear what kind of non-linearity is present, we expect to observe a strong amplitude component at $|f_1 - f_2|$ similar to $|f_1 + f_2|$. After applying the LPM, we notice that this component actually is present but was disguised by the transient. This is also apparent from the large change in phase after applying the LPM. Note that, the phase behavior over radius can seem counter-intuitive, however, it is important to realize that the non-linearity is modifying its behaviour significantly (see details [31]). Moreover, the difference frequency component $|f_1 - f_2|$ is not only present, it has exactly the same trend and a similar value as the component at $|f_1 + f_2|$. This suggests that non-linearity is static, at least for this frequency region.

The effect of transients is not so significant for the harmonic components f_1, f_2, and $f_1 + f_2$. The errors due to transients are additive meaning they are a summed with the perturbation. Consequently, it is most interesting to study the absolute errors due to transients. These errors are shown in Fig. 4 (bottom) and for completeness also the errors are shown for the perturbed frequencies $2f_1$ and $2f_2$. Note that, the error due to a transient is decreasing with increasing frequency and the same holds for increasing radius. This is expected as the transient decreases with increasing frequency as it consists of smooth trends which are inherently dominant at low frequency. Moreover, as transport over space is reducing the amplitude of all harmonic components, this also holds for the transient. The amplitude error of f_1 and f_2 is also increasing and is sometimes even larger than that of $|f_1 - f_2|$. This is due to the source not being perfectly periodic and can be observed in the spectra of the ECH waveforms (see [31]). As a consequence, the surrounding harmonic components of f_1 and f_2 contain also a small perturbation. This leads to a so-called skirt around f_1 and f_2 and makes the LPM compensation more difficult. In Fig. 2 and Fig. 3, this can be recognized by the "valley" between f_1 and f_2 not being at noise level. As such the LPM estimate will have a larger error here as it has trouble distinguishing this smooth curve from the actual transient. This can in general be avoided by using a higher frequency resolution, i.e., more periods. Also note that in Fig. 4 for "high" frequencies $2f_1$, $|f_1 + f_2|$, and $2f_2$, there is

not much error. This is because there is hardly any transient error at this frequency and we are close to the noise level here of approximately $4 \cdot 10^{-4}$ keV.

To summarize, this section shows an experimental application of the LPM to heat pulse propagation experiments showing the harmonic components in the output signal can be isolated by removing the approximated transient. This is particularly evident for the difference frequency which has been reconstructed correctly without using any information of the other perturbed harmonics or using spatial correlation. As expected the application of the LPM becomes less important with increasing frequency. Note that, the LPM can also be used to calculate the variance of the corrected harmonic components using the over-determination of the polynomial fit. However, due to the limited amount of information available, that is, only two full joint periods, any variance estimate would be unreliable. In the next section, application for the correction of transients in gas-puffing modulation experiments.

4. Emission front movement due to gas puff

This section presents the application of the LPM for gas-puffing experiments. The aim of the experiment is to derive a transfer function model to design a feedback controller to control the C-III emission front. The aim of the controller is to control the C-III emission front with the hope that we can control the degree of detachment where detachment is defined by the loss of total pressure along the field lines from upstream to the target resulting in the reduction of the total particle flux to the target plates. In these two presented experiments we were unable to reach detachment, even though, it was possible to derive a C-III emission front control model using the methodology presented here. This enabled us to control the C-III emission front. The feedback control experiments are not part of this work, see for details [36]) and corresponding journal article (to be published). As written, we focus on the control model derivation for control of the C-III emission front. For this it is necessity to apply the local polynomial method (LPM) on experimental data derived under challenging conditions, e.g., low signal-to-noise ratio (SNR), limited measurement time, and slow trends in measurements also called drifts. First, the experiment is introduced briefly, the effect of the LPM on the amplitude, phase, and confidence bounds of the estimated frequency response function is discussed.

4.1. H-mode gas-puffing experiments: background and setup

One of the challenges for future fusion devices is the mitigation of the heat and particle load on the divertor tiles. Without precaution, the resulting heat load will exceed the engineering limit of 10 $\mathrm{MW/m^2}$ [37]. One of the proposed solutions is plasma detachment [38], where neutral (impurity) gas puffing in the divertor ultimately leads to low heat and particle flux to the divertor target, preventing excessive erosion of the wall material. Detachment requires active feedback control to prevent reattachment and/or core confinement degradation [39]. Various experiments have been carried out on a wide range of machines, relying on the real-time interpretation of different plasma diagnostics such as Langmuir probes, bolometry, and thermocouples [40, 41, 42, 43]. Furthermore, in carbon wall machines, the onset of detachment is often associated with C-III 465 nm radiation line extinguishing near the divertor target [44]. This C-III emission front can be tracked in real-time by processing images originating from a multi-spectral imaging diagnostic [45, 46], allowing feedback control of the gas puff [36]. In this section, we focus on the derivation of the control model for gas-puff to the C-III emission front.

Typically in the field of high-tech systems, a feedback controller is designed offline to avoid time and cost consuming iterative methods. However, this requires dynamical detachment models, which are currently not (yet) available from first principles. Another way of deriving such a model is by means of perturbations (system identification) on the actual machine and discharge. The approach to analyze and design such experiments is covered in this section.

The experiments are carried out on the tokamak á configuration variable (TCV), in high-confinement mode (H-mode). H-mode is characterized by steep gradients in plasma density and temperature near the edge. During an edge localized mode (ELM) the large density and temperature gradient are driven unstable resulting in a large expulsion of particles and heat that are released into the scrape-off-layer. This collapse relaxes the gradients and this whole process often periodically repeats itself. This causes a high-frequent disturbance on the measurement of the emission front location. For this particular scenario on TCV, before perturbing the radiation front is moved from the target to a certain distance from the target. This state is reached around 0.8 s , leaving approximately 0.8 s for the system identification experiment. Furthermore, the actuator, the gas valve described in [47], has a limited bandwidth of approximately 50 Hz. This bandwidth is determined by the closing of the valve which has a significantly larger time-constant compared to the

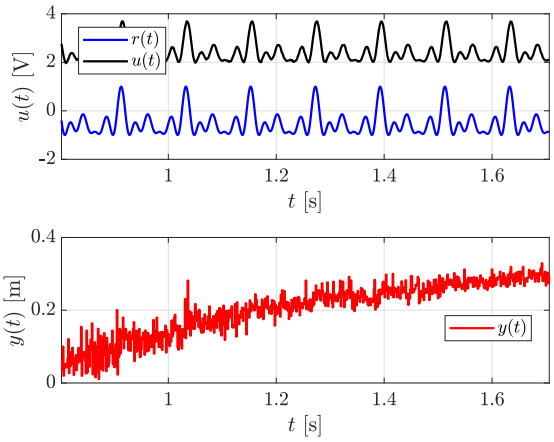

Figure 5. *color online* Time traces of the system identification experiment #65312. (top) the reference voltage for the gas valve $r(t)$, the gas valve outlet pressure sensor voltage $u(t)$ and (bottom) the distance from the target to the C-III emission front location $y(t)$ which is slowly moving away from the target.

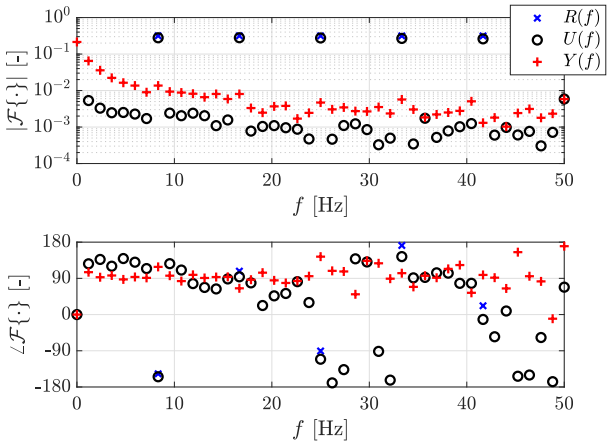

Figure 6. *color online* Bode diagram of the system identification experiment #65312 over the interval $t \in [0.8660, 1.7059]$. The excited frequencies in the input signals are well above the noise level, while the excited frequencies in the output spectrum $Y(f) = \mathcal{F}\{y(t)\}$ are clearly affected by the slow change of the emission front and are close to the noise level.

opening of the valve. Since there is no detachment controller yet, the perturbation $r(t)$ is applied on top of the existing constant feed-forward signal to the gas valve controller. The gas valve uses an internal feedback control system to regulate the outlet pressure sensor voltage $u(t)$ to match the desired input voltage. The constant feed-forward signal causes the emission front $y(t)$ to move upwards. This leads to a trend of the front location in the time domain. The combined effect of ELMs, the drift-like movement of the emission front, and short experimental time lead to limited measurement data with low SNR and a drift on the output signal. ELMs do not directly influence the measurements as for these discharges the smallest inter-time between ELMs is 12 ms (80 Hz) which is well above 50 Hz which is analyzed here. However, still we observe a worse SNR during ELMs which could be due to aliasing and lost frames due to overexposure.

The time signals and the Bode diagram for such experiments are shown in Fig. 5 and Fig. 6, respectively. The input signals $r(t)$, $u(t)$ are captured at a frequency of 500 Hz and the output signal $y(t)$ is captured at 800 Hz.

The presented time traces as well as the Fourier spectrum show that the input signal has a high SNR since the excited frequencies can be clearly distinguished from the noise.

The effect of transient behavior is limited, since the amplitude of the Fourier coefficients on the non-excited frequencies is almost flat. This is also a strong suggestion that there is no significant change in equilibrium due to a changing operating point (non-linearity) during the experiment: the presence of such an equilibrium change would manifest itself as higher amplitude Fourier coefficients at non-excited frequencies [20]. However, the output signal clearly has a low SNR. In the time domain, the response to the input signal is difficult to recognize. In the spectrum of the output signal, the excited frequencies are difficult to distinguish from the noise and transient/drift. The gradual drift of the emission front manifests itself in decaying amplitude of the Fourier spectrum for low frequencies, while the noise corresponds with the flat spectrum of the non-excited frequencies. Thus the first two excited frequencies are affected by the emission front drift, while all frequencies are affected by noise it is especially visible at higher frequencies.

As such, direct derivation of a frequency response function from this measurement data will result in an inaccurate approximation of the actual system dynamics. Application of the LPM to remove the transient response leads to an improved approximation of the frequency response given the available measurement time and actuator constraints. We will show the benefit of this method to the presented experiments in the coming section.

4.2. Application of the local polynomial method to reduce the effect of trends in the emission front

Since the input signal has a SNR around 60 dB, the LPM is only applied on the output signal, i.e., the measurement of the emission front location. The LPM works in a similar fashion as presented in the previous Sec. 3, but now only corrects the excited frequencies. The corrected Fourier coefficients of the output are divided by the Fourier coefficients of the reference signal to obtain the frequency response function at

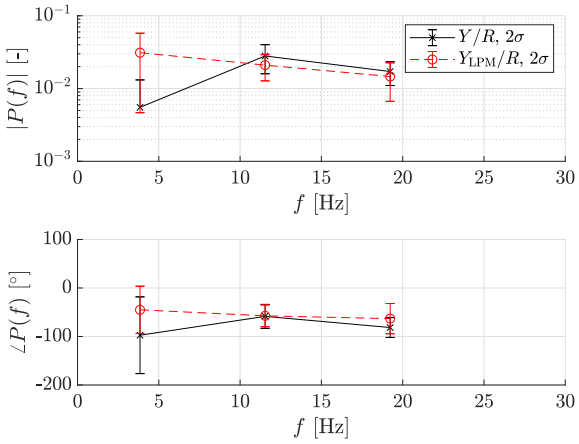

Figure 7. *color online* The different estimated frequency response functions from system identification experiment #65309 over the interval $t \in [0.9200, 1.6999]$. (top) The absolute value of the frequency response function and (bottom) the phase (i.e. angle) of the frequency response function. For each excited frequency, the 2σ confidence bound is given.

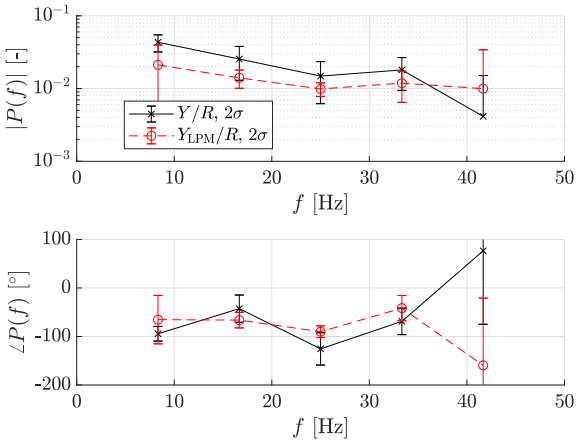

Figure 8. *color online* The different estimated frequency response functions from the system identification experiment #65312 over the interval $t \in [0.8660, 1.7059]$. (top) The absolute value of the frequency response function and (bottom) the phase (i.e. angle) of the frequency response function. For each excited frequency, the 2σ confidence bound is given. Note that if a confidence bound does not have a lower bound, this means that the confidence bound goes all the way to (through) zero, which cannot be displayed on a logarithmic scale.

the excited frequencies. Results from two different experiments are presented in Fig. 7 and Fig. 8.

There is a clear difference between the frequency response functions with and without the application of the LPM. For both data sets, the effect is clearly visible on both the amplitude and phase. For TCV discharge #65309, the LPM applies a major correction on the Fourier coefficients for the first excited frequency, resulting in a significant change on the amplitude and phase. For discharge #65312, the LPM corrections are more moderate. However, the overall characteristic of the phase changes significantly. Without the application of the LPM, the phase goes up and down over the first three excited frequencies, while after the application of LPM, the phase changes consistently for these three frequencies. As expected the dynamics to be smooth over frequencies as there is no theory that predicts resonances in these dynamics. Note that, not only the amplitude but also the phase is corrected in both directions (additive). This correction is caused similarly to the changes caused on the amplitude as explained in Sec. 3 and visualized in Fig. 2 and Fig. 3.

4.3. Confidence bounds on frequency response function estimates

Since the LPM determines the contribution of noise and drifts/transients on the Fourier coefficients, it is capable to also estimate the variance on the corrected output signal [48]. This variance is estimated based on the residue of the fit of the local polynomial method. As such, this variance can be used to determine the confidence bounds on the frequency response function.

Since the input signal has a sufficiently high SNR, the variance on the frequency response function on the excited frequencies f_{exc} can be approximated by

$$\begin{aligned} \hat{G}(f_{\mathrm{exc}}) &= \frac{Y_{\mathrm{LPM}}(f_{\mathrm{exc}})}{R(f_{\mathrm{exc}})} \\ \hat{\sigma}^2_{\hat{G}}(f_{\mathrm{exc}}) &\approx \frac{\hat{\sigma}^2_{Y_{\mathrm{LPM}}}(f_{\mathrm{exc}})}{|R(f_{\mathrm{exc}})|}, \end{aligned} \tag{6}$$

under the assumption that the noise is complex circular normal distributed [26]. The 2σ confidence bounds for both methods are also shown in Fig. 7 and Fig. 8. Note that the confidence bounds of the frequency response function where the LPM is applied are in general much smaller than the one without the LPM [48]. However, the variance at the lowest and highest excited frequency determined with LPM are larger than the one obtained without LPM since the variations in the surrounding frequencies are much higher than for the other frequencies.

The confidence bounds for #65312 are also numerically presented in Table 1. Note that the confidence bounds are only to be interpreted as the variation of the Fourier coefficient of the emission front measurement and does not include any errors in the measurement and calibration errors. A discussion on the source of such errors is highlighted in [46].

To summarize, this section shows the necessity of applying LPM on experimental data obtained under non-ideal conditions (e.g. with transients, drifts and low SNR). Without the application of LPM, trends (or transients) have a large influence on the

Table 1. Estimated variance of discharge #65312 for the excited frequency of both methods.

f_{exc}	$\hat{\sigma}^2_{Y/R}$	$\hat{\sigma}^2_{Y_{\text{LPM}/R}}$
08.333	$0.326 \cdot 10^{-4}$	$0.848 \cdot 10^{-4}$
16.667	$0.389 \cdot 10^{-4}$	$0.384 \cdot 10^{-5}$
25.000	$0.186 \cdot 10^{-4}$	$0.108 \cdot 10^{-5}$
33.333	$0.185 \cdot 10^{-4}$	$0.730 \cdot 10^{-5}$
41.667	$0.301 \cdot 10^{-4}$	$0.146 \cdot 10^{-3}$

Fourier coefficients, resulting in a frequency response function which does not describe the dynamical system adequately.

We have not validated the LPM with respect to the original spectrum (with the exception of confidence bound calculations). This validation can be done by comparing the data to a frequency response function without a transient and as has been done simulation, see e.g. [21, 22, 23]). However, such frequency response functions are not available experimentally here. What can be validated is that applying the LPM results in a frequency response function that is smoother over both amplitude and phase, which is not an assumption of the LPM. This is also what we expect from the physics as we are unaware of any models which predict strong fluctuations of the frequency response function over frequency for this type of gas perturbations. Technically, this is not a proper validation but shows that the LPM is working appropriately.

The LPM corrects for trends and measurement noise resulting in a frequency response function closer to the real dynamics. Although, in this particular case, the controller design would be stable even in the presence of wrong phases and amplitude in the frequency response function, there are most definitely cases imaginable where Bode's stability conditions seem not to be fulfilled due to wrongfully determined Fourier coefficients. Removing the transient reduces in general the variation of the Fourier coefficient over periods, as such the LPM can reduce the variance of the estimated Fourier coefficients. However, in case that a local polynomial cannot be fitted well, the confidence bounds will increase as the estimate of the Fourier coefficient is less reliable (as the residue of the fit is used to estimate the variance). Hence, the confidence bounds of the LPM have a relationship to the Fourier coefficients of the original signal but can be reduced if the LPM is successful but can also increase if a local polynomial cannot be used to estimate the transient.

5. Conclusion and discussion

In this paper, we presented a novel technique to correct for non-periodic behaviour in perturbative measurements used for physics interpretation and transfer function estimation for controller design. We have shown that non-periodic components lead to complex additive errors. Moreover, we have shown that, as long as there is a clear periodic component in the perturbative experiment, it is possible to remove transients and arrive at spectra with reduced error including confidence bounds. We have also shown that the local polynomial method can be adapted to take other non-periodic components into account in this case the non-linear components. In principle, this could also be used to compensate for (core) sawtooth, ELMs, and other periodic disturbances. However, in case of strongly fluctuating periods this would mean to exclude a range of frequency rather than a specific frequency. Finally, the examples presented here show the value of this approach which is especially important in the case of short experiments (timewise) and strong trends which are very common in perturbative fusion experiments.

Acknowledgments The authors thank J. Koenders and Dr. O. Février for their input on the manuscript and Dr. O. Février for his assistance during the TCV experiments.

This work has been carried out within the framework of the EUROfusion Consortium and has received funding from the Euratom research and training programme 2014-2018 and 2019-2020 under grant agreement No 633053. The views and opinions expressed herein do not necessarily reflect those of the European Commission. LHD ECRH system is supported under grants ULRR701, ULRR801, ULRR804 by NIFS. This work was supported in part by the Swiss National Science Foundation.

References

[1] Lopes Cardozo N J 1995 *Plasma Phys. Control. Fusion* **37** 799
[2] Ryter F, Dux R, Mantica P and Tala T 2010 *Plasma Phys. Control. Fusion* **52** 124043
[3] Mantica P and Ryter F 2006 *C. R. Physique* **7** 634
[4] Tardini G *et al.* 2009 *Nucl. Fusion* **49** 085010
[5] Bruhn C *et al.* 2018 *Plasma Phys. Control. Fusion* **60** 085011
[6] Ryter F *et al.* 2003 *Nucl. Fusion* **43** 1396
[7] Inagaki S *et al.* 2011 *Phys. Rev. Lett.* **107**(11) 115001
[8] Inagaki S *et al.* 2006 *Nucl. Fusion* **46** 133
[9] DeBoo J *et al.* 2012 *Phys. Plasmas* **19** 082518
[10] Salmi A *et al.* 2014 Gas puff modulation experiments in JET L- and H-mode plasmas *Proceedings of the 41st EPS Conference on Plasma Physics* vol 38F
[11] Tamura N *et al.* 2007 *Nucl. Fusion* **47** 449
[12] Faitsch M *et al.* 2017 *Plasma Phys. Control. Fusion* **59** 095006
[13] Hennen B 2011 *PhD Thesis*
[14] Hennen B, Westerhof E, Nuij P, De Baar M and Steinbuch M 2012 *Nucl. Fusion* **52** 074009
[15] Witvoet G, De Baar M, Westerhof E, Steinbuch M and Doelman N 2011 *Nucl. Fusion* **51** 073024
[16] The Mathworks, Inc. Natick, Massachusetts 2001 *Signal Processing Toolbox: User's Guide Version 5*

[17] Poularikas A D 2018 *Discrete Random Signal Processing and Filtering Primer with MATLAB* (Boca Raton: CRC Press)

[18] Stranneby D and Walker W 2004 *Digital Signal Processing and Applications* (Amsterdam; Boston; London: Elsevier)

[19] Mallat S 2009 *A Wavelet Tour of Signal Processing. The Sparse Way* (Burlington: Academic Press)

[20] Pintelon R and Schoukens J 2012 *System Identification: A Frequency Domain Approach* (Hoboken: John Wiley & Sons)

[21] Monteyne G, Vandersteen G, Pintelon R and Ugryumova D 2013 *Measurement* **46** 2210

[22] Voorhoeve R, Van der Maas A and Oomen T 2018 *Mech. Syst. Signal Process.* **105** 129

[23] Van der Maas R, Van der Maas A, Voorhoeve R and Oomen T 2017 *IEEE Trans. Control Syst. Technol.* **25** 1724

[24] Pintelon R, Schoukens J, Vandersteen G and Barbé K 2010 *Mech. Syst. Signal Process.* **24** 573

[25] Pintelon R, Schoukens J, Vandersteen G and Barbé K 2010 *Mech. Syst. Signal Process.* **24** 596

[26] Van Berkel M *et al.* 2014 *Plasma Phys. Control. Fusion* **56** 105004

[27] Geerardyn E and Oomen T 2017 *Control Eng. Pract.* **68** 63

[28] Peumans D, Busschots C, Vandersteen G and Pintelon R 2018 *IEEE Trans. Instrum. Meas.* **67** 1749

[29] Evers E, De Jager B and Oomen T 2018 *IFAC-PapersOnLine* **51** 808

[30] Pintelon R, Vandersteen G, Schoukens J and Rolain Y 2011 *Mech. Syst. Signal Process.* **25** 2892

[31] Van Berkel M *et al.* 2017 *Nucl. Fusion* **57** 126036

[32] Iiyoshi A *et al.* 1999 *Nucl. Fusion* **39** 1245

[33] Suzuki C *et al.* 2012 *Plasma Phys. Control. Fusion* **55** 014016

[34] Wambacq P and Sansen W 1998 *Distortion Analysis of Analog Integrated Circuits* vol 451 (Boston: Springer Science & Business Media)

[35] Takahashi H *et al.* 2014 *Phys. Plasmas* **21** 061506

[36] Ravensbergen T *et al.* 2020 *28th meeting of ITPA Topical Group SOL and Divertor Physics (DivSOL), Jan 13–16 2020, Jeju island, Korea*

[37] Loarte A *et al.* 2007 *Nucl. Fusion* **47** S203–S263

[38] Leonard A W 2018 *Plasma Phys. Control. Fusion* **60** 044001

[39] Lipschultz B, Parra F I and Hutchinson I H 2016 *Nucl. Fusion* **56** 056007

[40] Guillemaut C *et al.* 2017 *Plasma Phys. Control. Fusion* **59** 045001

[41] Kallenbach A *et al.* 2010 *Plasma Phys. Control. Fusion* **52** 055002

[42] Eldon D, Kolemen E, Humphreys D, Hyatt A, Järvinen A, Leonard A, McLean A, Moser A, Petrie T and Walker M 2019 *Nucl. Mater. Energy* **18** 285

[43] Wu K *et al.* 2018 *Nucl. Fusion* **58** 056019

[44] Theiler C *et al.* 2017 *Nucl. Fusion* **57** 072008

[45] Perek A *et al.* 2019 *Rev. Sci. Instrum.* **90** 123514

[46] Ravensbergen T, Van Berkel M, Silburn S A, Harrison J R, Perek A, Vijvers W A J, Theiler C, Kirk A and De Baar M R 2020 *accepted to Nucl. Fusion*

[47] Bates S C and Burrell K H 1984 *Rev. Sci. Instrum.* **55** 934

[48] Pintelon R, Barbé K, Vandersteen G and Schoukens J 2011 *Mech. Syst. Signal Process.* **25** 2683